Active and Reactive Power Control for Wind Turbine Based on a MIMO 2-Sliding Mode Algorithm With Variable Gains

Carolina Evangelista, Fernando Valenciaga, and Paul Puleston

***Abstract*—This study proposes a power control strategy for a grid-connected variable-speed wind turbine, based on a doubly-fed induction generator (DFIG) with slip power recovery. The control objectives vary with the zones of operation (dependant on the wind speed), aiming to maximize the active power in the *partial load* zone and to limit it when operating within the *full load* zone, while regulating the stator reactive power following grid requirements. The control design, based on the second-order sliding modes (SOSM) and Lyapunov, uses a modified version of the *super-twisting* algorithm with variable gains which can be applied to nonlinear multiple inputs–multiple outputs (MIMO) systems. The well-known robustness of the sliding techniques, the simplicity of the algorithm, and the adaptive characteristic of its gains are used together in this study to obtain a controller able to deal robustly with the exacting challenges presented by these systems. An additional benefit of the proposal lies in the smoothness of the control action, an important issue regarding applied mechanical efforts. Representative results obtained by simulation of the controlled system are shown and discussed.**

***Index Terms*—Energy conversion, power control, second-order sliding modes (SM), variable gains, wind power generation.**

I. Introduction

THE increasing energy demand, together with the harmful effect of fossil fuel exploitation on the climate and on the environment, are among the main factors that have boosted worldwide interest in renewable energies. Among them, wind energy is one of the options that has received the strongest impulses. The total global installed wind capacity has been growing significantly during the past few decades, reaching 239 GW by the end of 2011, accounting for 3% of the total world's electric consumption [1].

Research and technological development of wind energy conversion systems (WECS) play a decisive role in this growth, both focused on optimizing the efficiency of the system and on reducing loads and mechanical efforts, thus increasing its reliability and service life. Some of the most important subjects of interest are the search for new materials and turbine designs, the improvement of electronic sensors, the inclusion of stochastic processing techniques to estimate parameters of interest, and the use and development of advanced control techniques [2]–[5]. Regarding the latter, variable structure control techniques and their sliding modes (SM) arise as a suitable option for systems like these, which are based on a random source like the wind, exhibit a nonlinear behavior, and operate in highly disturbed environments. Among the several characteristics of the SM control, the most interesting to be mentioned in this application are the following [6]–[8].

1) The designs can be realized using linear or nonlinear models, and there are algorithms for SISO (single input–single output) as well as for MIMO systems.
2) The resulting controllers are usually simple and easy to implement, and they require low computational burden while operating in real time.
3) The controlled systems result robust to several kinds of external and internal disturbances, and to certain variations in the parameters.

A power control strategy is developed in this study for a variable-speed WECS topology based on a doubly fed induction generator (DFIG) and connected to the grid with a twofold objective, stator reactive power regulation, and extracted power optimization, or regulation according to the zone of operation. The second-order sliding modes (SOSM) MIMO with variable gains strategy is based on a reelaboration of the theoretical approach presented by Dávila *et. al* [9]. The final design combines the advantages of the SOSM techniques regarding robustness and simplicity in implementation and operation, together with the beneficial reduction of mechanical efforts in a wider range of operation associated with the adaptive characteristic of the variable gains of the controller.

II. Brief Description of the System

This study focuses on one of the most popular configurations nowadays regarding grid-connected variable-speed WECS, which is based on a DFIG. In particular, it consists of a wound rotor induction generator connected to the grid directly through the stator and by means of a bidirectional power electronic system through the rotor windings. This topology is presented schematically in Fig. 1.

This system can work at variable speed, generating and delivering electrical power at the frequency and voltage fixed by

Manuscript received November 26, 2012; revised April 16, 2013; accepted June 18, 2013. Date of current version August 16, 2013. This work was supported in part by the Consejo Nacional de Investigaciones Cientìficas y Técnicas (CONICET) and Universidad Nacional de La Plata (UNLP) (Argentina), and in part by the Marie Curie FP7-2011-IIF, ACRES (299767/911767) (EU). Paper no. TEC-00623-2012.

The authors are with the Facultad de Ingeniería, Universidad Nacional de La Plata, La Plata 1900, Argentina and also with Consejo Nacional de Investigaciones Cientìficas y Técnicas, Buenos Aires C1033AAJ, Argentina (e-mail: cae@ing.unlp.edu.ar; fval@ing.unlp.edu.ar; puleston@ing.unlp.edu.ar).

Color versions of one or more of the figures in this paper are available online at http://ieeexplore.ieee.org.

Digital Object Identifier 10.1109/TEC.2013.2272244

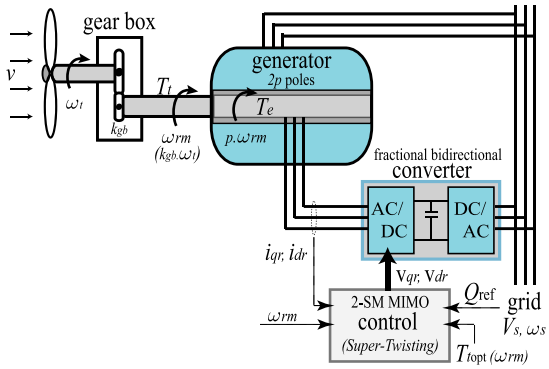

Fig. 1. WECS-DFIG configuration.

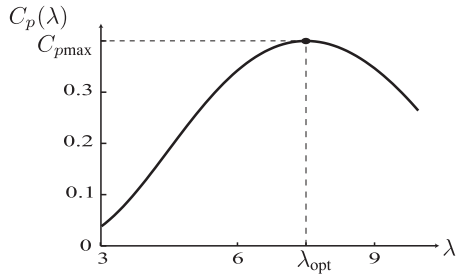

Fig. 2. Power coefficient: $C_p(\lambda) = c_1(c_2/\lambda - 1)e^{-c_3/\lambda}$.

the grid. The DFIG can be operated in both sub- and super-synchronous speeds by electronically controlling the converter. In the second mode, electrical power is fed to the grid through both the stator and the rotor, whereas when operating subsynchronously, electrical power is delivered into the rotor from the grid (bidirectional converter). As only the rotor power is fed through the electronic converter, the latter has to manage only a fraction of the power production, thus resulting in smaller size and less cost than in other configurations. Its nominal power determines the rotor speed variation range around the rated speed [2], [10]. It is worth mentioning that, being a topology with slip power recovery, it is possible to generate more power than the nominal of the generator.

The mechanical power a wind turbine can capture, P_t, is a fraction of the available power in the wind ($P_\nu = 0.5\pi\rho R^2\nu^3$) and it can be written as [11]

$$P_t = P_\nu\, C_p(\lambda, \beta_P) = 0.5\pi\rho R^2 C_p(\lambda, \beta_P)\nu^3 \qquad (1)$$

where ν represents the wind speed, rho is the air density, R is the blade length, and C_p is the power coefficient of the turbine, which depends on the shape and the geometry of the blades. This coefficient is a nonlinear function of the pitch angle of the blades, β_P, and the tip speed ratio, $\lambda = \frac{\omega_{\rm rm} R}{k_{\rm gb}\,\nu}$, where $\omega_{\rm rm}$ is the mechanical rotation speed of the generator rotor and $k_{\rm gb}$ the gear box relation (a rigid drive train is assumed). When the pitch angle is maintained fixed, the C_p has a unique maximum, for $\lambda = \lambda_{\rm opt}$ as it can be seen in Fig. 2.

Regarding power generation, two regions can be distinguished in the useful operation range of the turbine. They depend on the wind speed and require different control objectives, as it is indicated in Fig. 3 [11].

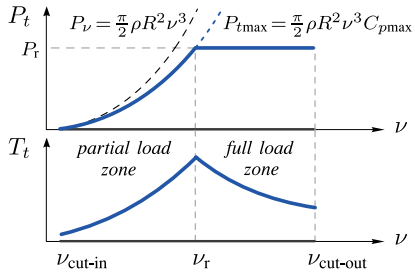

Fig. 3. Power and torque in the useful zones of operation for a wind turbine.

Within the *partial load zone*, between $\nu_{\rm cut\text{-}in}$ (minimum wind speed at which the turbine starts generating) and the rated speed $\nu_{\rm r}$, it is desirable to maximize the extraction of the energy available in the wind. The control in this zone is usually performed electronically, maintaining the pitch angle fixed. The other useful region, known as the *full load zone*, is defined between ν_r and $\nu_{\rm cut\text{-}out}$ (limit wind speed, up from which the turbine should be turned off to prevent damages). Within this zone the extraction of power is limited to the rated value, which can be accomplished by controlling either the pitch angle of the blades or the electrical variables of the DFIG.

A. Reduced Dynamic Model

The dynamic behaviour of the WECS-DFIG can be accurately described by a five-order set of differential equations. Four of them account for the electrical dynamics of the induction machine viewed from two quadrature reference frames rotating at synchronic speed, one for the rotor variables and the other for the stator ones. In terms of the machine fluxes, they can be expressed as

$$\begin{cases} \dot{\phi}_{ds} &= \mathrm{v}_{ds} - R_s i_{ds} + \omega_s \phi_{qs} \\ \dot{\phi}_{qs} &= \mathrm{v}_{qs} - R_s i_{qs} - \omega_s \phi_{ds} \\ \dot{\phi}_{dr} &= \mathrm{v}_{dr} - R_r i_{dr} + (\omega_s - p\,\omega_{\rm rm})\phi_{qr} \\ \dot{\phi}_{qr} &= \mathrm{v}_{qr} - R_r i_{qr} - (\omega_s - p\,\omega_{\rm rm})\phi_{dr} \end{cases} \qquad (2)$$

with the following algebraic relations:

$$\begin{aligned} \phi_{ds} &= L_s i_{ds} + L_m i_{dr} \\ \phi_{qs} &= L_s i_{qs} + L_m i_{qr} \\ \phi_{dr} &= L_r i_{dr} + L_m i_{ds} \\ \phi_{qr} &= L_r i_{qr} + L_m i_{qs} \end{aligned} \qquad (3)$$

where the variables ϕ_{ds}, ϕ_{qs}, ϕ_{dr} and ϕ_{qr} represent the quadrature components of the stator and rotor concatenated flux components, v_{ds}, v_{qs}, v_{dr} and v_{qr} (i_{ds}, i_{qs}, i_{dr} and i_{qr}) are the quadrature components of the stator and rotor winding voltages (currents). Moreover, ω_s is the frequency of the grid (in rad/s), p is the number of pole pairs, R_s and R_r represent the electric resistances of the stator and rotor windings respectively, L_s and L_r are the self-inductances of the windings, and L_m is the mutual inductance between windings.

The fifth equation accounts for the mechanical dynamics of the rotating parts, which can be given by

$$\dot{\omega}_{\rm rm} = \frac{1}{J}\left(T_t - T_e\right) \tag{4}$$

where J represents the inertia of the whole rotating parts, T_e is the electrical resistant torque of the generator, and T_t is the torque produced by the wind on the blades (referred to the high speed shaft by means of the gear box relation constant). The torques can be expressed as

$$T_e = \frac{3}{2} p L_m \left(i_{qs} i_{dr} - i_{ds} i_{qr}\right) \tag{5}$$

$$T_t = \frac{1}{k_{\rm gb}} 0.5 \pi \rho R^3 C_t\left(\lambda\right) \nu^2 \tag{6}$$

where $C_t(\lambda)$ is the torque coefficient of the turbine, defined as $C_p(\lambda)/\lambda$.

Making some geometrical and electrical considerations, regarding the relative alignment between the rotating frames and the spatial fluxes, and neglecting the stator resistance, the WECS description given previously can be simplified, allowing to obtain a reduced-order model more adequate for the control design process [12], [13]. This description consists of three differential equations accounting for the electrical dynamics of the rotor and the dynamics of the mechanical rotational speed

$$\begin{aligned}\dot{i}_{qr} = &-\left(\frac{L_m V_s}{L_e} + \omega_s i_{dr}\right)\left(1 - \frac{p}{\omega_s}\omega_{\rm rm}\right) \\ &- \frac{R_r L_s}{L_e} i_{qr} + \frac{L_s}{L_e} \mathrm{v}_{qr}\end{aligned} \tag{7}$$

$$\dot{i}_{dr} = \omega_s i_{qr}\left(1 - \frac{p}{\omega_s}\omega_{\rm rm}\right) - \frac{R_r L_s}{L_e} i_{dr} + \frac{L_s}{L_e}\mathrm{v}_{dr} \tag{8}$$

$$\dot{w}_{\rm rm} = \frac{1}{J}\left(T_t(\nu, \omega_{\rm rm}) - \frac{3 p L_m V_s}{2 \omega_s L_s} i_{qr}\right) \tag{9}$$

where V_s is the grid line voltage and $L_e = L_s L_r - L_m^2$. The stator currents can be algebraically calculated knowing the rotor currents

$$\begin{aligned} i_{qs} &= -\frac{L_m}{L_s} i_{qr} \\ i_{ds} &= \frac{V_s}{\omega_s L_s} - \frac{L_m}{L_s} i_{dr.}\end{aligned} \tag{10}$$

When the machine is operating on the points where the power extraction is maximum ($C_p = C_{p\max}$, $\lambda = \lambda_{\rm opt}$), the corresponding torque can be expressed as a function of the squared rotational speed

$$T_{\rm opt}(\omega_{\rm rm}) = \frac{\pi \rho R^5 C_{p\max}}{2 k_{\rm gb}^3 \lambda_{\rm opt}^3} \omega_{\rm rm}^2 \;=\; k_o \omega_{\rm rm}^2 \tag{11}$$

with $k_o = \frac{\pi \rho R^5 C_{p\max}}{2 k_{\rm gb}^3 \lambda_{\rm opt}^3}$. On the other hand, when the wind speed is high and the generation of power is limited to the rated, the corresponding torque depends directly on this value, P_r, and inversely on the rotational speed, i.e.,

$$T_r(\omega_{\rm rm}) = \frac{P_r}{\omega_{\rm rm}}. \tag{12}$$

Both cases are depicted in Fig. 3.

Finally, the stator reactive power can be expressed as

$$Q_s = \frac{3 V_s^2}{2 \omega L_s} - \frac{3 L_m V_s}{2 L_s} i_{dr}. \tag{13}$$

The proposal in this study fulfills two simultaneous objectives for each operation mode. A control strategy is designed to accomplish both of them simply, robustly, and avoiding unnecessary mechanical efforts. One of the aims contributes to compensate the reactive power needs of the grid, by regulating the stator reactive power following an external reference. The other involves the extraction of power and varies with the zone of operation:

1) Within the *partial load zone* the aim is to maximize the extracted power, controlling the points of operation so that $T_e = T_{\rm opt}$ for all wind speeds in this zone.
2) In the *full load zone* the extracted power is limited to the rated power of the machine. This objective is accomplished by maintaining the resistant torque equal to $P_r/\omega_{\rm rm}$ when $\omega_{\rm rm}$ exceeds the rated speed.

III. Controller

A. Second-Order Sliding Modes (2-SM)

The idea of the 2-SM control techniques is to zero a function of the system's states, the sliding variable σ, and its first time derivative, $\dot{\sigma}$. The function is designed based on the desired control objectives, to guarantee their achievement when $\sigma = 0$. The condition $\sigma = \dot{\sigma} = 0$ determines the 2-sliding manifold in the state space. A 2-SM algorithm acts taking the trajectories in the state space to the 2-sliding manifold and keeping them operating on it, i.e., makes the system operate in 2-SM.

There are several 2-SM algorithms, each of them with their own characteristics. In particular, the *super-twisting* algorithm [14] has a quite simple law and allows to synthesize a continuous control action with discontinuous time derivative, which makes the trajectories reach the 2-sliding manifold in finite time and robustly maintains the 2-SM operation. Encouraging results have been obtained applying this algorithm, with constant gains, to diverse configurations of WECS [12], [15]. New advanced techniques based on this algorithm have been explored in [16], where a SISO *super-twisting* controller with variable gains was developed for a rather simple SISO configuration of a WECS, and compared with a fixed-gains design. The auspicious conclusions emerged there motivated the proposal in this study.

The advantage of the present proposal lies in the wider range of operation and in the smoothness of the MIMO control action, both associated with the variability of the controller gains. A continuous and smooth control action results in great interest in these systems, as the induced mechanical stress is low. Besides, the MIMO algorithm does not imply a significant increase in the implementation complexity. Therefore, the computational burden is low during the online operation of the controller.

B. Controller Design

The components of the sliding variable are chosen as follows, to achieve the desired control objectives when operating in 2-SM

regime

$$\sigma_1 = T_{\rm ref} - T_e = T_{\rm ref}(\omega_{\rm rm}) - \frac{3pL_m V_s}{2\omega_s L_s} i_{qr} \tag{14}$$

$$\sigma_2 = Q_{\rm ref} - Q_s = Q_{\rm ref}(t) + \frac{3L_m V_s}{2L_s}\left(i_{dr} - \frac{V_s}{\omega_s L_m}\right) \tag{15}$$

where $Q_{\rm ref}$ is the external reference for the reactive power, determined by the grid needs, and $T_{\rm ref}$ is the torque reference, which varies between two functions depending on the zone of operation

$$T_{\rm ref}(\omega_{\rm rm}) = \begin{cases} T_{\rm opt} = k_o \omega_{\rm rm}^2, & \omega \le \omega_{\rm rm_r} \\ T_{\rm r} = \dfrac{P_r}{\omega_{\rm rm}}, & \omega \ge \omega_{\rm rm_r.} \end{cases} \tag{16}$$

In order to work with a set of variables containing the two sliding variables, a change of variables is made at this point. The third variable is chosen to be the mechanical rotation speed. After the change, the dynamics of the new variables [errors and mechanical of system (7)–(9)] can be written as

$$\begin{aligned} \dot\sigma_1 = {} & \frac{1}{J}(T_t - T_{\rm ref} + \sigma_1)\, T_{\rm ref}^{'} + \frac{R_r L_s}{L_e}(T_{\rm ref} - \sigma_1) \\ & + p\left(1 - \frac{p}{\omega_s}\omega_{\rm rm}\right)\left(\sigma_2 - Q_{\rm ref} + \frac{3L_r V_s^2}{2\omega_s L_e}\right) \\ & \underbrace{-\frac{3pL_m V_s}{2\omega_s L_e}\mathrm{v}_{qr}}_{u_1} = F_1(\sigma, \omega_{\rm rm}, t) + u_1 \end{aligned} \tag{17}$$

$$\begin{aligned} \dot\sigma_2 = {} & \frac{\omega_s^2}{p}\left(1 - \frac{p}{\omega_s}\omega_{\rm rm}\right)(T_{\rm ref} - \sigma_1) - \frac{3R_r V_s^2}{2\omega_s L_e} \\ & - \frac{R_r L_s}{L_e}(\sigma_2 - Q_{\rm ref}) + \dot{Q}_{\rm ref} + \underbrace{\frac{3L_m V_s}{2L_e}\mathrm{v}_{dr}}_{u_2} = \\ = {} & F_2(\sigma, \omega_{\rm rm}, t) + u_2 \end{aligned} \tag{18}$$

$$\dot\omega_{\rm rm} = \frac{1}{J}(T_t - T_{\rm ref} + \sigma_1) = F_3(\sigma, \omega_{\rm rm}, t) \tag{19}$$

where $T_{\rm ref}^{'}$ is the partial derivative of $T_{\rm ref}$ with respect to its argument, $\omega_{\rm rm}$

$$T_{\rm ref}^{'}(\omega_{\rm rm}) = \begin{cases} 2k_o\omega_{\rm rm}, & \omega \le \omega_{\rm rm_r} \\ -\dfrac{P_{\rm r}}{\omega_{\rm rm}^2}, & \omega \ge \omega_{\rm rm_r.} \end{cases} \tag{20}$$

Then, the dynamics can be written in the general form

$$\dot\sigma_{1,2} = \underbrace{f_{1,2}(\sigma, \omega_{\rm rm}, t) + \tilde f_{1,2}(\sigma, \omega_{\rm rm}, t)}_{F_{1,2}(\sigma, \omega_{\rm rm}, t)} + u_{1,2} \tag{21}$$

$$\dot\omega_{\rm rm} = \underbrace{f_3(\sigma, \omega_{\rm rm}, t) + \tilde f_3(\sigma, \omega_{\rm rm}, t)}_{F_3(\sigma, \omega_{\rm rm}, t)}. \tag{22}$$

In the previous equations, functions f represent the nominal or unperturbed model and their expressions are the ones of functions $F(\cdot)$ in (17)–(19) using the nominal values for all the parameters. On the other hand, functions $\tilde f$ account for measuring and modeling errors, uncertainties in the parameters and external disturbances. To obtain expressions for them, the propagated errors are computed from (17)–(19), after writing the variations of the parameters with respect to their nominal values in a separate way.

Each component of the control action is proposed to be computed as the addition of two terms

$$u_i = u_{\mathrm{eq}_i} + \tilde u_i \tag{23}$$

where $u_{\mathrm{eq}_{1,2}}$ are the equivalent control for (21) unperturbed and $\tilde u_{1,2}$ are designed using a variant of a version of the *super-twisting* algorithm developed in [9], with variable gains and applicable to MIMO systems.

The expressions for the equivalent control terms are obtained solving u algebraically from the equations formed by equalling to zero the first time derivative of σ, (21), with $\tilde f = 0$. Thus, $u_{\mathrm{eq}_i} = -f_i$.

On the other hand, the expression for each component $\tilde u_i,\ i = 1, 2$, is proposed as

$$\begin{aligned} \tilde u_i = {} & -k_{1i}(\sigma_1, \sigma_2, \omega_{\rm rm}, t)\phi_{1i}(\sigma_i) \\ & - \int_0^t k_{2i}(\sigma_1, \sigma_2, \omega_{\rm rm}, \tau)\phi_{2i}(\sigma_i) d\tau \end{aligned} \tag{24}$$

$$\phi_{1i}(\sigma_i) = k_{ci}|\sigma_i|^{\frac{1}{2}}\mathrm{sign}(\sigma_i) \tag{25}$$

$$\phi_{2i}(\sigma_i) = \phi_{1i}^{'}(\sigma_i)\phi_{1i}(\sigma_i) = \frac{k_{ci}^2}{2}\mathrm{sign}(\sigma_i) \tag{26}$$

where $\phi_{1i}^{'}(\sigma_i)$ is the partial derivative of ϕ_{1i} with respect to σ_i, and $k_{ci} > 0$ is a constant. The design of the variable gains $k_{1i}(\cdot)$ and $k_{2i}(\cdot)$ is based on Lyapunov (see Section III-C), and it requires to divide each function $\tilde f_i(\sigma, \omega_{\rm rm}, t)$ into two additive terms $\tilde f_i = g_{1i} + g_{2i}$:

$$g_{2i}(\omega_{\rm rm}, t) = \tilde f_i(0, \omega_{\rm rm}, t) \tag{27}$$

$$g_{1i}(\sigma, \omega_{\rm rm}, t) = \tilde f_i(\sigma, \omega_{\rm rm}, t) - g_{2i}(\omega_{\rm rm}, t) \tag{28}$$

where the functions g_{2i} account for the perturbations on the 2-SM manifold, and the g_{1i} consider the remaining errors. Then, continuous functions $\varrho_{ji}(\sigma, \omega_{\rm rm}, t) \ge 0$ have to be found so that the perturbations can be bounded as

$$|g_{1i}(\sigma, \omega_{\rm rm}, t)| \le \varrho_{1i}(\sigma, \omega_{\rm rm}, t)|\phi_{1i}(\sigma_i)| \tag{29}$$

$$\left|\frac{d}{dt} g_{2i}(\omega_{\rm rm}, t)\right| \le \varrho_{2i}(\sigma, \omega_{\rm rm}, t)|\phi_{2i}(\sigma_i)|. \tag{30}$$

Under these conditions, the finite-time convergence to the 2-SM manifold and the robustness against all disturbances and errors considered in functions $\tilde f$ are guaranteed if the variable gains k_{1i} and k_{2i} in (24) are computed as

$$\begin{aligned} k_{1i}(\sigma, \omega_{\rm rm}, t) = {} & \delta_i + 1/\beta_i\big[(2\epsilon_i\varrho_{1i} + \varrho_{2i})^2/(4\epsilon_i) + \epsilon_i \\ & + 2\epsilon_i\varrho_{2i} + (2\epsilon_i + \varrho_{1i})(\beta_i + 4\epsilon_i^2)\big] \end{aligned} \tag{31}$$

$$k_{2i}(\sigma, \omega_{\rm rm}, t) = \beta_i + 4\epsilon_i^2 + 2\epsilon_i k_{1i} \tag{32}$$

where β_i, ϵ_i, and δ_i are positive arbitrary constants.

A block diagram of the controller is presented in Fig. 4.

To determine the bounding functions (29)–(30) for this system, a thorough analysis was performed on the equations of

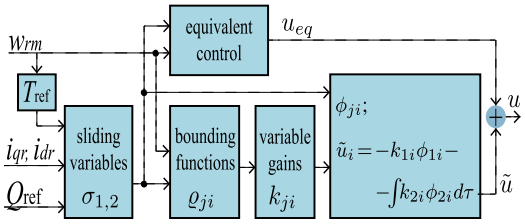

Fig. 4. Diagram of the proposed controller.

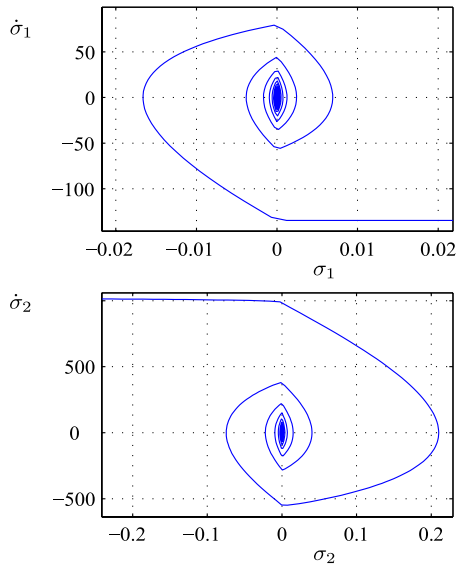

Fig. 5. Convergence in the planes σ_i–$\dot{\sigma}_i$ (design model used in simulations).

the model, together with physical considerations on the realistic conditions of operation and the assistance of comprehensive computer simulations. Several wind speed profiles were used in the simulations and several reactive power references were tested, in order to consider a wide variety of situations with the system operating in the range of the two zones of interest. In addition, certain external disturbances and parameter errors were taken into account through the whole procedure, such as given next.

1) Variations in the electrical resistances and in the electromagnetic inductances up to $\pm 10\%$ of their respective rated values.
2) Variations from the rated values of the electrical grid parameters: up to $\pm 10\%$ in the voltage and up to $\pm 2\%$ in the angular frequency.

The values of the parameters for the controllers was finely adjusted with the aid of new simulations, and the final choices were the following:

$$\begin{aligned} k_{c1} &= 25; \quad \epsilon_1 = 10^{-5}; \quad \delta_1 = 10^{-4}; \quad \beta_1 = 1000 \\ k_{c2} &= 51; \quad \epsilon_2 = 10^{-8}; \quad \delta_2 = 10^{-4}; \quad \beta_2 = 1000. \end{aligned} \tag{33}$$

It would be illustrative to show the convergence of the state trajectories to the MIMO 2-SM plane, using the design model. However, this is not possible, due to the number of dimensions of the required graphic. The convergence is shown separately, instead, at the origin of the two planes σ_i–$\dot{\sigma}_i$ (see Fig. 5).

C. Stability Analysis

The system given by (21)–(22) and controlled by (23)–(26), as described in Section III-B, can be rewritten as

$$\begin{cases} \dot{\omega}_{\rm rm} = f_3(\sigma, \omega_{\rm rm}, t) + \tilde{f}_3(\sigma, \omega_{\rm rm}, t) \\ \dot{\sigma}_i = g_{1i}(\sigma, \omega_{\rm rm}, t) - k_{1i}(\sigma, \omega_{\rm rm}, t)\phi_{1i}(\sigma_i) + z_i \\ \dot{z}_i = \dfrac{d}{dt} g_{2i}(\omega_{\rm rm}, t) - k_{2i}(\sigma, \omega_{\rm rm}, t)\phi_{2i}(\sigma_i). \end{cases}$$

Then, the following function of the states can be proposed as the Lyapunov candidate:

$$V = \sum_{i=1}^{2} V_i \; = \; \zeta_1^T \mathrm{P}_1 \zeta_1 + \zeta_2^T \mathrm{P}_2 \zeta_2. \tag{34}$$

Each term corresponds to the proposals given in [9] and [17], i.e.,

$$\zeta_i^T = [\phi_{1i}(\sigma_i);\; z_i] = [k_{ci}|\sigma_i|^{1/2}\mathrm{sign}(\sigma_i);\; z_i] \tag{35}$$

$$\mathrm{P}_i = \mathrm{P}_i^T = \begin{bmatrix} \beta_i + 4\epsilon_i^2 & -2\epsilon_i^2 \\ -2\epsilon_i^2 & 1 \end{bmatrix} > 0 \tag{36}$$

if β_i, ϵ_i, and δ_i are positive constants.

The steps of the general proof, and the particular one developed for a single control variable in [16] are followed here to show that $\dot{V} < 0$. Then, the time derivative of each term V_i is calculated as $\dot{\zeta}_i^T \mathrm{P}_i \zeta_i + \zeta_i^T \mathrm{P}_i \dot{\zeta}_i$. If for the perturbation functions in (27) and (28) there are functions α_{1i} and α_{2i} such that the following expressions can be written:

$$g_{1i}(\sigma, \omega_{\rm rm}, t) = \alpha_{1i}(\sigma, \omega_{\rm rm}, t)\, \phi_{1i}(\sigma_i) \tag{37}$$

$$\frac{d}{dt} g_{2i}(\omega_{\rm rm}, t) = \alpha_{2i}(\sigma, \omega_{\rm rm}, t)\, \phi_{2i}(\sigma_i) \tag{38}$$

then, it is possible to write

$$\dot{\zeta}_i = \frac{d}{d\sigma}\phi_{1i}(\sigma)\, \mathrm{A}_i(\sigma, \omega_{\rm rm}, t)\, \zeta_i \tag{39}$$

$$\dot{V}_i = -\frac{d}{d\sigma}\phi_{1i}(\sigma)\, \zeta_i^T \mathrm{Q}_i(\sigma, \omega_{\rm rm}, t)\, \zeta_i \tag{40}$$

where $\mathrm{Q}_i = \mathrm{A}_i^T \mathrm{P}_i + \mathrm{P}_i \mathrm{A}_i$ is symmetric and

$$\mathrm{A}_i(\sigma, \omega_{\rm rm}, t) = \begin{bmatrix} k_{1i} - \alpha_{1i} & 1 \\ k_{2i} - \alpha_{2i} & 0 \end{bmatrix}.$$

At this point, the second variable gain is defined as in (32) to simplify expressions and it is supposed that continuous functions $\varrho_{ji}(\sigma, \omega_{\rm rm}, t) \geq 0$ can be found that verify $|\alpha_{ji}| \leq \varrho_{ji}$. It can be easily shown that the built matrix $(\mathrm{Q}_i - 2\epsilon_i \mathrm{I})$ is positive definite, with I the identity matrix of size 2, if the first variable gain is defined as in (31). With this result, (40) can be bounded as

$$\dot{V}_i \leq -2\epsilon_i \frac{d}{d\sigma}\phi_{1i}(\sigma)\|\zeta_i\|_2^2 = -\frac{\epsilon_i k_{ci}^2}{|\sigma_i|^{1/2}}\|\zeta_i\|_2^2 \tag{41}$$

where $\|\cdot\|_2^2$ is the square of the 2-norm (Euclidean). Working on this expression and using the standard inequality for quadratic forms $\lambda_{mi}\|\zeta_i\|_2^2 \leq \zeta_i^T \mathrm{P}_i \zeta_i = V_i \leq \lambda_{Mi}\|\zeta_i\|_2^2$, where λ_{Mi} and

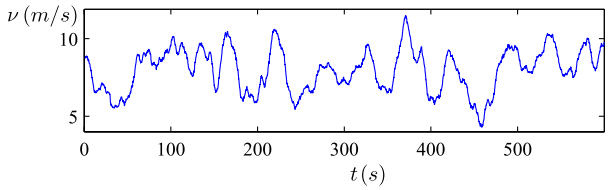

Fig. 6. Wind speed profile.

λ_{mi} are the maximum and minimum eigenvalues of matrix $\mathrm{P}_i > 0$, it can be stated

$$V_i^{\frac{1}{2}} \geq \lambda_{mi}^{1/2} \|\zeta_i\|_2 \geq \lambda_{mi}^{1/2} k_{ci} |\sigma_i|^{1/2} \tag{42}$$

given that the norm of a vector is greater than any of its components. Using these results in (41), it is found that

$$\dot{V}_i \leq -\frac{\epsilon_i k_{ci}^2 \lambda_{mi}^{1/2}}{\lambda_{Mi}} V_i^{\frac{1}{2}} = \gamma_i V_i^{\frac{1}{2}} \tag{43}$$

where $\gamma_i = \frac{\epsilon_i k_{ci}^2 \lambda_{mi}^{1/2}}{2\lambda_{Mi}} > 0$. Finally, the total time derivative of V can be bounded as

$$\dot{V} \leq -\gamma_1 V_1^{\frac{1}{2}} - \gamma_2 V_2^{\frac{1}{2}} \leq 0 \tag{44}$$

taking the zero value only in the equilibrium $(\sigma, z) = \mathbf{0}$. Thus, it can be concluded that the latter is globally stable.

Then, to state that the 2-SM manifold is reached in finite time from any initial condition, a new looser bound is found for the derivative of $V_i\,(\sigma_i(t), z_i(t))$ of the form $\dot{V}_i \leq -aV_i^{1/2} - bV_i$, working analogously as when determining (43). In this condition, the comparison principle [18] can be applied, as it gives the conditions to bound the solution of a scalar differential inequality with the continuous solution of a differential equation. In this sense, the solution of $\dot{u}(t) = -au^{1/2} - bu$, found to be $u(t) = \left(\frac{a}{b} - ce^{-tb/2}\right)^2$, with c constant, overbounds $V_i\,(\sigma_i(t), z_i(t))$. As $u(t)$ reaches zero in time $T = \frac{2}{b}\ln\left(\frac{bc}{a}\right)$, then V_i is zeroed in a time less or equal than T as well, and so do the variables $\sigma_i(t)$ and $z_i(t)$.

Regarding the system's zero dynamics, given by (19), it can be shown to be stable on the sliding manifold in both zones. In this way, when working in the *partial load zone*, the rotational speed converges to the one corresponding to the optimal working point $\omega_{\mathrm{rm}} = \frac{\lambda_{\mathrm{opt}} k_{\mathrm{gb}}}{R}\nu$.

IV. Simulations and Results

Representative results are shown and discussed in this section. The final design for the proposed control strategy, developed using the reduced-order model, was finally assessed by simulation using a complete model of the WECS-DFIG given by (2)–(4) and subjected to disturbances. The simulations were run for 10-min periods with the system working under realistic conditions in both zones of operation. The nominal values of the parameters used in the simulations are listed in the Appendix.

The wind speed profile is depicted in Fig. 6.

The temporal evolution of the electrical parameters (resistances, inductances, grid voltage, and frequency), varying from their nominal values, are depicted in Figs. 7 and 8, respectively.

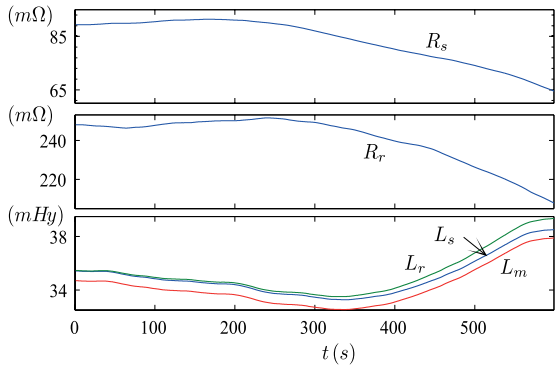

Fig. 7. Temporal evolution of the electromagnetic parameters of the generator.

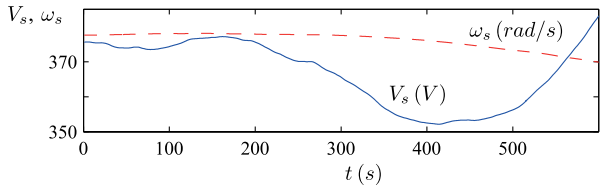

Fig. 8. Temporal evolution of the grid parameters.

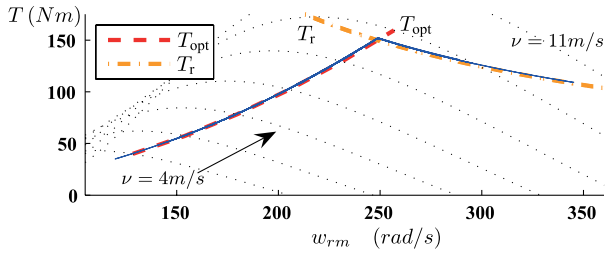

Fig. 9. T_e versus ω_{rm} in the torque–speed plane, where the reference torques T_{opt} and T_{r} are also shown. The turbine characteristics T_t–ω_{rm} are shown in dotted lines for various wind speeds.

The instant values are unknown for the controller, but they fulfil the bounds considered in the design stage.

The variations of the electric torque of the generator T_e versus the rotational speed w_{rm} are shown in the torque–speed plane in Fig. 9. The figure also presents the reference curve for each zone of operation (partial/full load), indicated T_{opt} and T_r, respectively. As it can be appreciated, the designed controller manages to maintain the generator torque equal to the reference in both zones, despite the disturbances and parameters variations, satisfying the first proposed objective.

The active power curves are presented in Fig. 10. In particular, the rated power P_{r} the maximum extractable power from the wind $P_{t\max}$, and the actual extracted power P_t, are shown in dotted, red dashed, and blue solid lines, respectively. The two expected behaviors can be identified, according to the zone of operation: $P_{t\max}$ lower or greater than P_{r}. As it can be noted, the tracking is very good but not exact. The main reason for this lies in the control strategy used to accomplish the proposed objectives: when an optimum torque reference is used, the extracted power follows the maximum power filtered by the mechanical dynamics.

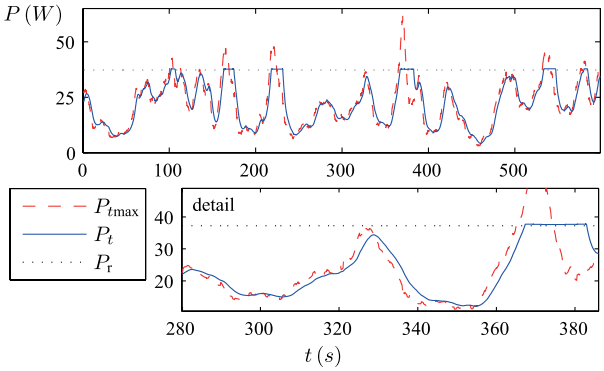

Fig. 10. Maximum extractable power (red dashed), rated power (black dotted), and captured power (solid blue). Lower box: detail of the above.

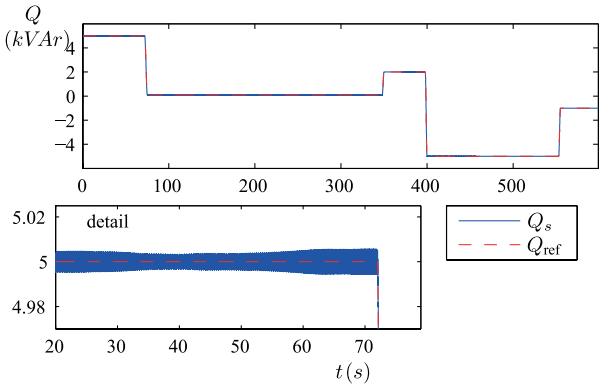

Fig. 11. Stator reactive power and its reference (they are overlapped). Lower box: detail of the above.

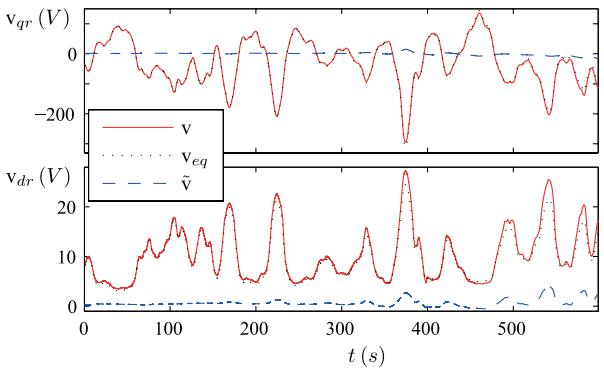

Fig. 12. Control voltages v_{qr} and v_{dr}, and its corresponding components: $\mathrm{v}_{qr_{\mathrm{eq}}}$ and $\mathrm{v}_{dr_{\mathrm{eq}}}$ (based on the equivalent control), and $\tilde{\mathrm{v}}_{qr_{\mathrm{eq}}}$ and $\tilde{\mathrm{v}}_{dr_{\mathrm{eq}}}$ (*super-twisting* components).

The fulfillment of the second control objective can be appreciated in Fig. 11, where the stator reactive power and the external reference Q_{ref} are depicted together. The two curves are overlapped in the above box, showing the excellent tracking of the reference. As it can be observed in the lower box, the error is quite small, remaining below 1% during the simulations.

Fig. 12 presents the control inputs, the rotor voltages v_{qr} (upper box), and v_{dr} (lower box), both in red solid lines. The two constituent terms of each component are also shown in the figure, separately: v_{eq} in black dotted line and $\tilde{\mathrm{v}}$ in blue dashed line. It is noticeable that the terms based on the equivalent control are

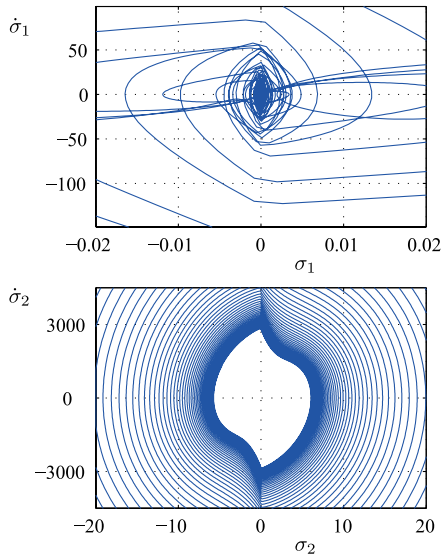

Fig. 13. Convergence in the planes σ_i–$\dot{\sigma}_i$ (using complete model).

larger and are more influential in the control action. On the other hand, the terms based on the *super-twisting* algorithm, smaller, are in charge of compensating for the disturbances, errors in the models and variations in the parameters, and providing robustness. In this sense, it can be appreciated that this components grow a little larger in the second half of the simulation time, when the disturbances grow (see Figs. 6–8). It is important to highlight the smoothness of the control signals.

Finally, the convergence of the state trajectories to the MIMO 2-SM plane is illustrated in Fig. 13, at the origin of the two planes σ_1–$\dot{\sigma}_1$ and σ_2–$\dot{\sigma}_2$. The effect of the increase in the order of the dynamics is noticeable when comparing these curves with the ones obtained in the design stage (shown previously in Fig. 5) [19], [20]. It can be seen that the origin of the plane σ_2–$\dot{\sigma}_2$ is not reached exactly in this case, existing a smooth oscillation in σ_2. These variations are small, ranging between $\pm 5.10^{-3}$ kVAr when $Q_{\mathrm{ref}} = 5$ kVAr, representing a tracking error of 0.1%.

V. Conclusion

A MIMO power control strategy based on SOSM was presented here for a grid-connected variable-speed wind energy conversion system with slip power recovery. Two main objectives were aimed at and accomplished simply, robustly, and avoiding unnecessary mechanical efforts. One of them involved the regulation of the stator reactive power (contributing to compensate the grid power factor) and the other, the control of the extracted power from the wind (maximizing or limiting it, according to the zone of operation).

Specifically, a Lyapunov-based variation of the *super-twisting* algorithm with variable gains and applicable to nonlinear MIMO systems was used to design the proposed controller. In addition to the robustness of the *super-twisting* algorithm, the variability of the controller gains in this proposal allows having a wider range of operation with a smooth control action, maintaining an excellent performance and with no significant increase in the algorithm complexity. A reduced model of the WECS

was considered for the design stage, in order to simplify the computations.

A candidate Lyapunov function was presented for the MIMO algorithm with variable gains. With this function it was possible to design the controller for the MIMO nonlinear system and to demonstrate the convergence of the algorithm, i.e., the convergence of the system states to sliding mode operation. At the same time, the proof established the robustness of the controller against several disturbances and uncertainties in the parameters.

To be able to guarantee robustness, an explicit expression of the disturbances, errors, and uncertainties had to be found and split into two, and two positive functions had two be found to bound them in a certain way. Although these calculations are not simple, they are made offline and only once (during the design and tuning stage). The online operation of the controllers is simple, with low computational burden and it requires the measuring of few system variables.

The resulting controller was tested afterward through extensive simulations using a realistic and disturbed full-order model. It was shown that the control objectives were successfully attained, performing robustly despite the considered disturbances and uncertainties, and the increase in the order of the system.

APPENDIX

NOMINAL PARAMETERS AND OTHER VALUES

$P_{\rm nom} = 50$ HP;	$\omega_s = 2\pi 60$ rad/s;	$V_s = 460\sqrt{2/3}$ V;
$L_s = 35.5$ mHy;	$L_r = 35.5$ mHy;	$L_m = 35.7$ mHy;
$R_r = 228$ mΩ;	$R_s = 82$ mΩ;	$p = 2$;
$J = 3.662$ Kgm^2;	$k_{\rm gb} = 25$;	$R = 7.3$ m;
$c_1 = 9.5946$;	$c_2 = 12$;	$c_3 = 20$;
$C_{p\max} = 0.4$;	$\lambda_{\rm opt} = 7.5$;	

REFERENCES

[1] (2012, Mar.). "Small wind world report 2012," World Wind Energy Association, Tech. Rep., [Online]. Available: http://www.wwindea.org/

[2] I. Munteanu, A. Bratcu, N. Cutululis, and E. Ceanga, *Optimal Control of Wind Energy Systems*. London, U.K.: Springer-Verlag, 2007.

[3] G. Nallavan, R. Dhanasekaran, and M. Vasudevan, "Power electronics in wind energy conversion systems—A survey across the globe," in *Proc. 3rd Int. Conf. Electron. Comput. Technol.*, 2011, pp. 416–419.

[4] A. Mesemanolis, C. Mademlis, and I. Kioskeridis, "High-efficiency control for a wind energy conversion system with induction generator," *IEEE Trans. Energy Convers.*, vol. 27, no. 4, pp. 958–967, Dec. 2012.

[5] D. Joshi and S. Jangamshetti, "A novel method to estimate the o&m costs for the financial planning of the wind power projects based on wind speed—A case study," *IEEE Trans. Energy Convers.*, vol. 25, no. 1, pp. 161–167, Mar. 2010.

[6] A. Sabanovic, L. M. Fridman, and S. Spurgeon, Eds., *Variable Structure Systems: From Principles to Implementation*. London, U.K.: IET, 2004.

[7] L. Fridman and A. Levant, *Sliding Mode Control in Engineering*. New York, NY, USA: Marcel Dekker, 2002, ch. 3, pp. 53–101.

[8] G. Bartolini, A. Levant, A. Pisano, and E. Usai, "2-sliding mode with adaptation," presented at the Proc. 7th IEEE Mediterranean Conf. Control and Automation, Haifa, Israel, 1999.

[9] A. Dávila, J. Moreno, and L. Fridman, "Variable gains Super-Twisting algorithm: A Lyapunov based design," presented at the 2010 Amer. Control Conf., Baltimore, MD, USA, Jun. 2010.

[10] A. M. Alkandari, S. A. Soliman, and M. H. Abdel-Rahman, "Steady state analysis of a doubly fed induction generator," *Energy Power Eng.*, vol. 3, pp. 393–400, Sep. 2011.

[11] T. Burton, D. Sharpe, N. Jenkins, and E. Bossanyi, *Wind Energy Handbook*. Chichester, U.K.: Wiley, 2001.

[12] B. Beltran, M. Benbouzid, and T. Ahmed-Ali, "Second-order sliding mode control of a doubly fed induction generator driven wind turbine," *IEEE Trans. Energy Convers.*, vol. 27, no. 2, pp. 261–269, Jun. 2012.

[13] F. Valenciaga and C. Evangelista, "2-sliding active and reactive power control of a wind energy conversion system," *IET Control Theory Appl.*, vol. 4, no. 11, pp. 2479–2490, Nov. 2010.

[14] A. Levant, "Sliding order and sliding accuracy in sliding mode control," *Int. J. Control*, vol. 58, no. 6, pp. 1247–1263, 1993.

[15] F. Valenciaga and P. F. Puleston, "High-order sliding control for a wind energy conversion system based on a permanent magnet synchronous generator," *IEEE Trans. Energy Convers.*, vol. 23, no. 3, pp. 860–867, Sep. 2008.

[16] C. Evangelista, P. Puleston, F. Valenciaga, and L. Fridman, "Lyapunov designed Super-twisting sliding mode control for wind energy conversion optimization," *IEEE Trans. Ind. Electron.*, vol. 60, no. 2, pp. 538–545, Feb. 2012.

[17] J. A. Moreno and M. Osorio, "A Lyapunov approach to second-order sliding mode controllers and observers," in *Proc. 47th IEEE Conf. Decis. Control*, Dec. 2008, pp. 2856–2861.

[18] H. Khalil, *Nonlinear Systems*, 3rd ed. Upper Saddle River, NJ, USA: Prentice—Hall, 2002.

[19] I. Boiko and L. Fridman, "Analysis of chattering in continuous sliding-mode controllers," *IEEE Trans. Autom. Control*, vol. 50, no. 9, pp. 1442–1446, Sep. 2005.

[20] M. K. Khan, S. K. Spurgeon, and A. Levant, "Simple output-feedback 2-sliding controller for systems of relative degree two," presented at the Eur. Control Conf., Cambridge, U.K. Sep. 2003

Carolina Evangelista received the Engineer's degree in electronics and the Ph.D. degree from the Universidad Nacional de La Plata (UNLP), La Plata, Buenos Aires, Argentina, in 2006 and 2012, respectively.

She is currently a Teaching Assistant at the Department of Electrical Engineering, UNLP, and holds a Postdoctoral position with the Consejo Nacional de Investigaciones Cientìficas y Técnicas and UNLP, Argentina. Her research interest includes second-order sliding mode control with applications to renewable energy systems.

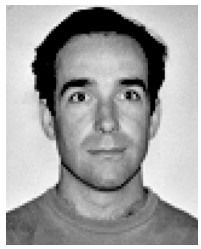

Fernando Valenciaga received the B.S.E.E. and Ph.D. degrees from the Universidad Nacional de La Plata (UNLP), La Plata, Buenos Aires, Argentina, in 1993 and 2001, respectively.

He is currently an Assistant Professor of Automatic Control at the Department of Electrical Engineering, UNLP. His research interests include automatic control systems and renewable energy systems.

Dr. Valenciaga is a Research Member of the Consejo Nacional de Investigaciones Cientìficas y Técnicas, Argentina.

Paul Puleston received the B.S.E.E. degree (with first class Hons.) and the Ph.D. degree from the Universidad Nacional de La Plata (UNLP), La Plat, Buenos Aires, Argentina, in 1988 and 1997, respectively.

He is currently a Professor at the Department of Electrical Engineering, UNLP and a Researcher of Consejo Nacional de Investigaciones Cientìficas y Técnicas, Argentina. His research interests include automatic control systems, theory, and applications.